



1

2 Raindrop Fall Velocities from an Optical Array Probe and 2D-Video
3 Disdrometer

4 Viswanathan Bringi¹, Merhala Thurai¹ and Darrel Baumgardner²

5 ¹ *Department of Electrical and Computer Engineering, Colorado State University, Fort*
6 *Collins, Colorado, USA*

7 ² *Droplet Measurements Technologies, Longmont, Colorado, USA*

8 Correspondence to: V.N. Bringi

9 Email: bringi@colostate.edu

10

11



12 Abstract

13 We report on fall speed measurements of rain drops in light-to-heavy rain events from
14 two climatically different regimes (Greeley, Colorado, and Huntsville, Alabama) using
15 the high resolution (50 microns) Meteorological Particle Spectrometer (MPS) and a 3rd
16 generation (170 microns resolution) 2D-video disdrometer (2DVD). To mitigate wind-
17 effects, especially for the small drops, both instruments were installed within a 2/3-scale
18 Double Fence Intercomparison Reference (DFIR) enclosure. Two cases involved light-
19 to-moderate wind speeds/gusts while the third case was a tornadic supercell that
20 passed over the site with high wind speeds/gusts. As a proxy for turbulent intensity,
21 maximum wind speeds from 10-m height at the instrumented site recorded every 3 s
22 were differenced with the 5-min average wind speeds and then squared. The fall speed
23 versus size from 0.1-2 mm were derived from the MPS data and the 2DVD was used for
24 sizes >0.7 mm. Consistency of fall speeds from the two instruments in the overlap
25 region (0.7-2 mm) gave confidence in the data quality and processing methodologies.
26 Our results indicate that under light-to-moderate wind gusts, the mean fall speeds agree
27 well with fits to the terminal velocity measured in the laboratory by Gunn and Kinzer
28 from 100 microns up to precipitation sizes. In the supercell case the very strong gusts
29 and inferred high turbulence intensity caused a significant broadening of the fall speed
30 distributions with the mean fall speeds about 25-30% less than the terminal velocity of
31 Gunn-Kinzer, i.e. sub-terminal fall speeds.

32

33



34 1 Introduction

35 Knowledge of the terminal fall speed of raindrops as function of size is important in
36 modelling collisional break-up and coalescence processes (e.g., *List et al.*, 1987), in the
37 radar-based estimation of rain rate, in retrieval of drop size distribution using Doppler
38 spectra at vertical incidence (e.g., *Sekhon and Srivastava*, 1971) and in soil erosion
39 studies (e.g., *Rosewell* 1986). The terminal velocity measurements of *Gunn and Kinzer*,
40 1949) under calm laboratory conditions, and fits to their data (e.g., *Atlas et al.*, 1973;
41 *Footo and du Toit*, 1969; *Beard and Pruppacher*, 1969) are still considered the standard
42 against which measurements using more modern optical instruments in natural rain are
43 compared (*Löffler-Mang and Joss*, 2000; *Barthazy et al.*, 2004; *Schönhuber et al.*, 2008;
44 *Testik and Rahman*, 2016). More recently, the broadening and skewness of the fall
45 speed distributions of a given size (3 mm) in one intense rain event was attributed to
46 mixed-mode amplitude oscillations (*Thurai et al.*, 2013). Super- and sub-terminal fall
47 speeds in intense rain shafts have been detected and attributed, respectively, to drop
48 breakup fragments (sizes < 0.5 mm), and high wind/gusts (sizes 1-2 mm) (*Montero-*
49 *Martinez et al.*, 2009; *Larsen et al.*, 2014; *Montero-Martinez and Garcia-Garcia*, 2016).

50 The fall speeds and concentration of small drops (< 1 mm) in natural rain are difficult to
51 measure given the poor resolution (>170 microns) of most optical disdrometers and/or
52 sensitivity issues. While cloud imaging probes (with high resolution 25-50 microns) on
53 aircraft have been used for many years they generally cannot measure the fall speeds.
54 A relatively new instrument, the Meteorological Particle Spectrometer (MPS) is a droplet
55 imaging probe that was built by Droplet Measurements Technologies (DMT, Inc.) under
56 contract from the US Weather Service specifically designed for drizzle as small as 50
57 μm and rain drops up to 3 mm. This instrument in conjunction with a lower resolution
58 2D-Video Disdrometer (*Schoenhuber et al.*, 2008) is used in this paper to measure fall
59 speed distributions in natural rain.

60 This paper briefly describes the instruments used, presents fall speed measurements
61 from two sites under relatively low wind conditions, and one case from an unusual
62 tornadic supercell with high winds and gusts and ends with a brief discussion and
63 summary of the results.

64

65 2 Instrumentation and Measurements

66 The principal instruments used in this study are the MPS and 3rd generation 2D-video
67 disdrometer (2DVD), both located within a 2/3-scale Double Fence Intercomparison
68 Reference (DFIR; *Rasmussen et al.*, 2012) wind shield. As reported in (*Notaros et al.*,
69 2016), the 2/3-scale DFIR was effective in reducing the ambient wind speeds by nearly



70 a factor of 2-3 based on data from outside and inside the fence. The flow field in and
71 around the DFIR has been simulated by (*Theriault et al.*, 2015) assuming steady
72 ambient winds. They found that depending on the wind direction relative to the
73 octagonal fence, weak up/down drafts could be generated above the sensor areas. For
74 5 m/s speeds, the up/down drafts could range between -0.4 (down) to 0.2 m/s (up).

75 The instrument set-up was the same for the two sites (Greeley, Colorado and
76 Huntsville, Alabama). Huntsville has a very different climate from Greeley, and its
77 altitude is 212 m MSL as compared with 1.4 km MSL for Greeley. According to the
78 Köppen–Trewartha climate classification system (*Trewartha and Horn*, 1980), this labels
79 Greeley as a semiarid-type climate, whereas Huntsville is a humid subtropical-type
80 climate (*Belda et al.*, 2014).

81 The MPS is an optical array probe (OAP) that uses the technique introduced by
82 *Knollenberg* (1970, 1976, 1980) and measures drop diameter in the range from 0.05-3.1
83 mm. A 64 element photo-diode array is illuminated with a 660 nm collimated laser
84 beam. Droplets passing through the laser cast a shadow on the array and the decrease
85 in light intensity on the diodes is monitored with the signal processing electronics. A two
86 dimensional image is captured by recording the light level of each diode during the
87 period that the array is shadowed. The fall velocity is derived using two methods. One
88 uses the same approach as described in (*Montero-Martinez et al.*, 2009) where the fall
89 velocity is calculated from the product of the true air speed clock and ratio of the image
90 height -to-width. Note that “width” is the horizontal dimension parallel to the array and
91 “height” is along the vertical. The second method computes the fall velocity from the
92 maximum horizontal dimension (spherical drop shape assumption) divided by the
93 amount of time that the image is on the array, a time measured with a 2 MHz clock. In
94 order to be comparable to the results of (*Montero-Martinez et al.*, 2009), their approach
95 is implemented here for sizes > 250 μm . The fall velocity of smaller, slower moving
96 droplets, are measured using the second technique.

97 The limitations and uncertainties associated with OAP measurements have been well
98 documented (*Korolev et al.*, 1991; 1998; *Baumgardner et al.*, 2017). All possible
99 corrections have been applied, including the removal of artifacts due to splashing, and
100 oversizing that results from out-of-focus droplets (*Korolev* 2007). The sizing and fall
101 speed errors primarily depend on the digitization error (± 25 microns). The fall speed
102 accuracy according to the manufacturer (DMT) is <10% for 0.25 mm and <1% for sizes
103 greater than 1 mm, limited primarily by the accuracy in droplet sizing.

104

105 The 3rd generation 2DVD is described in detail by (*Schoenhuber et al.*, 2007; 2008) and
106 its accuracy of size and fall speed measurement has been well documented (e.g.,



107 *Thurai et al.*, 2007; 2009; *Huang et al.*, 2008; *Bernauer et al.*, 2015). Considering the
108 horizontal pixel resolution of 170 microns and other factors, the effective sizing range is
109 $D > 0.7$ mm. The fall velocity accuracy is determined primarily by the accuracy of
110 calibrating the distance between the two orthogonal light “sheets” or planes and is $< 5\%$
111 for fall velocity < 10 m s⁻¹. In our application, we utilize the MPS for measurement of
112 small drops with $D < 1.2$ mm and to compare the measurements with the 2DVD in the
113 overlap region of $D \approx 0.7$ – 2.0 mm to ensure consistency of observations. The only fall
114 velocity threshold used for the 2DVD is the lower limit set at 0.5 m s⁻¹ in accordance
115 with the manufacturer guidelines for rain measurements.

116

117 2.1 Fall Speeds from Greeley, Colorado

118 We first consider a long duration (around 20 h) rain episode on 17 April 2015 which
119 consisted of a wide variety of rain types/rates (mostly light stratiform < 8 mm h⁻¹) as
120 described in Table 2 of (*Thurai et al.*, 2017). Two wind sensors at height of 1 m were
121 available to measure the winds outside and inside the DFIR. Average wind speeds
122 were, respectively, < 1.5 m s⁻¹ inside the DFIR and < 4 m s⁻¹ outside with light gusts.
123 These wind sensors were specific to the winter experiment described in (*Notaros et al.*,
124 2016) and were unavailable for the rain measurement campaign after May 2015.

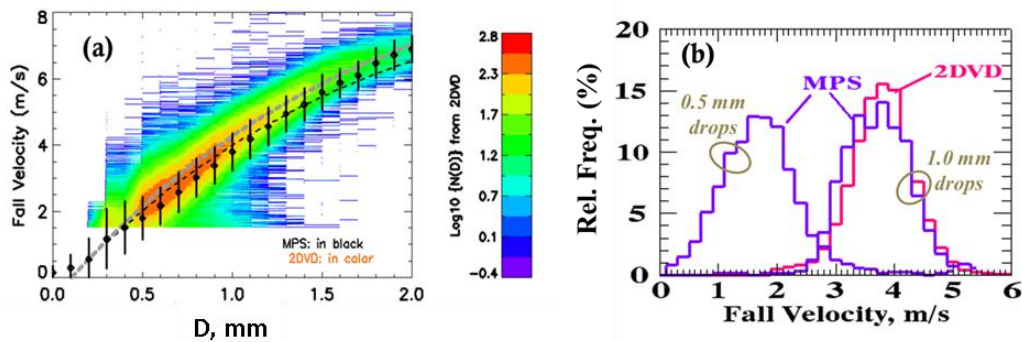
125 Figure 1(a) shows the fall speeds versus D from the 2DVD (shown as contoured
126 frequency of occurrence), along with mean and $\pm 1\sigma$ standard deviation from the MPS.
127 Also shown is the (*Atlas et al.*, 1973) fit to the terminal fall speed measurements of
128 (*Gunn and Kinzer*, 1949) at sea level and after applying altitude corrections (*Beard*,
129 1976) for the elevation of 1.4 km MSL for Greeley. Panel (b) shows the histogram of fall
130 speeds for two selected diameter intervals (0.5 ± 0.1 mm) and (1 ± 0.1 mm). Panel (a)
131 demonstrates the excellent “visual” agreement between the two instruments in the
132 overlap size range (0.7–2 mm) as well as with the fit to the Gunn-Kinzer laboratory data.
133 Notable is the remarkable agreement in mean fall speeds between the Gunn-Kinzer fit
134 and the MPS for $D < 0.5$ mm down to near the lower limit of the instrument (0.1 mm).
135 Few measurements have been reported of fall speeds in this size range.

136 The histograms in Fig. 1(b) show good agreement between 2DVD and MPS for 1 mm
137 drop sizes. The visual agreement between the two instruments is excellent with respect
138 to the mode, symmetry, spectral width and lack of skewness in the distributions. The
139 mean is 3.8 m s⁻¹ while the spectral width or standard deviation from MPS data is 0.6 m
140 s⁻¹. The corresponding coefficient of variation (ratio of standard deviation to mean) is
141 15.7% . The finite bin width (± 0.1 mm) used causes a “spread” of around 0.5 m s⁻¹ which
142 is clearly a significant contributor to the measured coefficient of variation. The definition
143 of sub- or super-terminal fall speeds by (*Montero-Martinez et al.*, 2009) is based on fall



144 speeds that are, respectively, less than 0.7 times the mean value or greater than 1.3
 145 times the mean value (i.e., exceeding 30% threshold on either side of the mean terminal
 146 fall speed). From examining the 1 mm size fall speed histogram there is negligible
 147 evidence of occurrences with fall speeds $<2.66 \text{ m s}^{-1}$ (sub) or $>4.94 \text{ m s}^{-1}$ (super).

148



149

150 *Figure 1.* (a) Fall velocity versus diameter (D). The contoured frequency of occurrence from
 151 2DVD data is shown in color (log scale). The mean fall velocity and $\pm 1\sigma$ standard deviation bars
 152 are from MPS. The dark dashed line is from the fit to the laboratory data of Gunn and Kinzer
 153 (1949) and the grey dashed line is the same except corrected for the altitude of Greeley, CO
 154 (1.4 km MSL). (b) Relative frequency histograms of fall velocity for the 0.5 ± 0.1 mm and
 155 1 ± 0.1 mm bins.

156

157 The histogram from MPS for the 0.5 mm sizes shows positive skewness with mean of
 158 1.8 m s^{-1} , spectral width of 0.65 m s^{-1} and corresponding coefficient of variation nearly
 159 doubling to 35%. The finite bin width (± 0.1 mm) causes a “spread” of 0.4 m s^{-1} which
 160 contributes to the measured coefficient of variation. Nevertheless, it is not possible to
 161 rule out the occurrence of sub- or super-terminal fall speeds, respectively, less than
 162 1.26 m s^{-1} or exceeding 2.34 m s^{-1} (i.e., exceeding 30% of the mean value) based on
 163 our data.

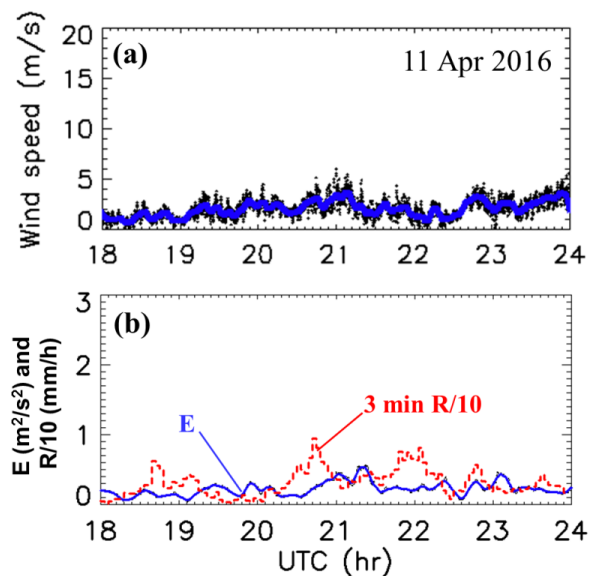
164

165 2.2 Fall Speeds from Huntsville, Alabama

166 The first Huntsville event occurred on 11 April 2016 and consisted of precipitation
 167 associated with the mesoscale vortex of a developing squall line that moved across
 168 northern Alabama between 1800 and 2300 UTC and produced over 25 mm of rainfall in
 169 the Huntsville area. Figure 2(a) shows the ambient 10-m height wind speeds (3 s and 5-



170 min averaged) recorded at the site. Maximum speeds were less than 5 m s^{-1} and wind
171 gusts were light. As no direct *in situ* measurement of turbulence was available we use
172 the approach by (Garrett and Yuter, 2014) who estimate the difference between the
173 maximum wind speed, or gust, that was sampled every 3 s, and the average wind
174 speed from successive 5 min intervals. The estimated turbulent intensity is proportional
175 to $E = (\text{Gusts} - \text{AverageWind})^2/2$. Figure 2(b) shows the E values which were small
176 (maximum $E < 0.4 \text{ m}^2 \text{ s}^{-2}$) indicative of low turbulence. Also, shown in Fig. 2(b) is the
177 2DVD-based time series of rainfall rate (R) averaged over 3 mins; the maximum R is
178 around 10 mm h^{-1} .



179

180 *Figure 2: (a) 3-s raw and 5-min averaged wind speeds at 10-m height. (b) turbulent*
181 *intensity estimates E , and 3-min averaged R (note: plot is $R/10$).*

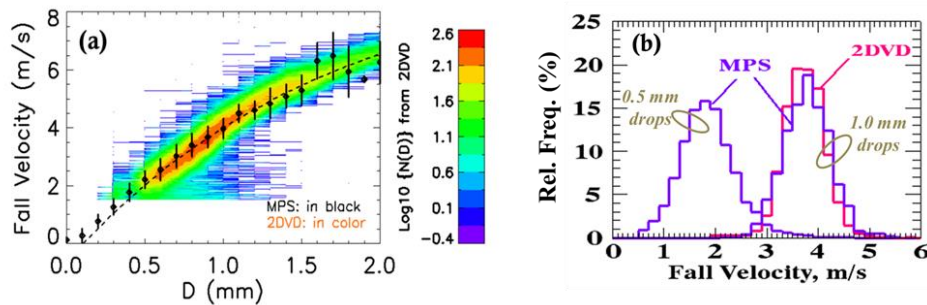
182

183 Figure 3(a) shows the fall velocity versus D comparison between the two instruments
184 while panel (b) shows the histograms for the 0.5 and 1 mm bins. Similar to the Greeley
185 event, the mean fall speed agreement between both instruments in the overlap region is
186 excellent and consistent with the fit to the Gunn-Kinzer laboratory data. As in Fig. 1(a),
187 the MPS data in Fig. 3(a) is in excellent agreement with Gunn-Kinzer fit for sizes < 0.5
188 mm.

189 The 0.5 and 1 mm histogram shapes in Fig. 3(b) are quite similar to the Greeley case
190 shown in Fig. 1(b). The mean and standard deviations from the MPS data for the 0.5
191 and 1 mm bins are, respectively, $[2 \ 0.62]$ and $[3.88 \ 0.44] \text{ m s}^{-1}$. The comments made



192 earlier with respect to Fig. 1(b) of the Greeley event are also applicable here. In
193 particular, the fall speed histogram for the 0.5 mm sizes cannot rule out the occurrence
194 of sub- or super-terminal fall speeds based on our data.



195

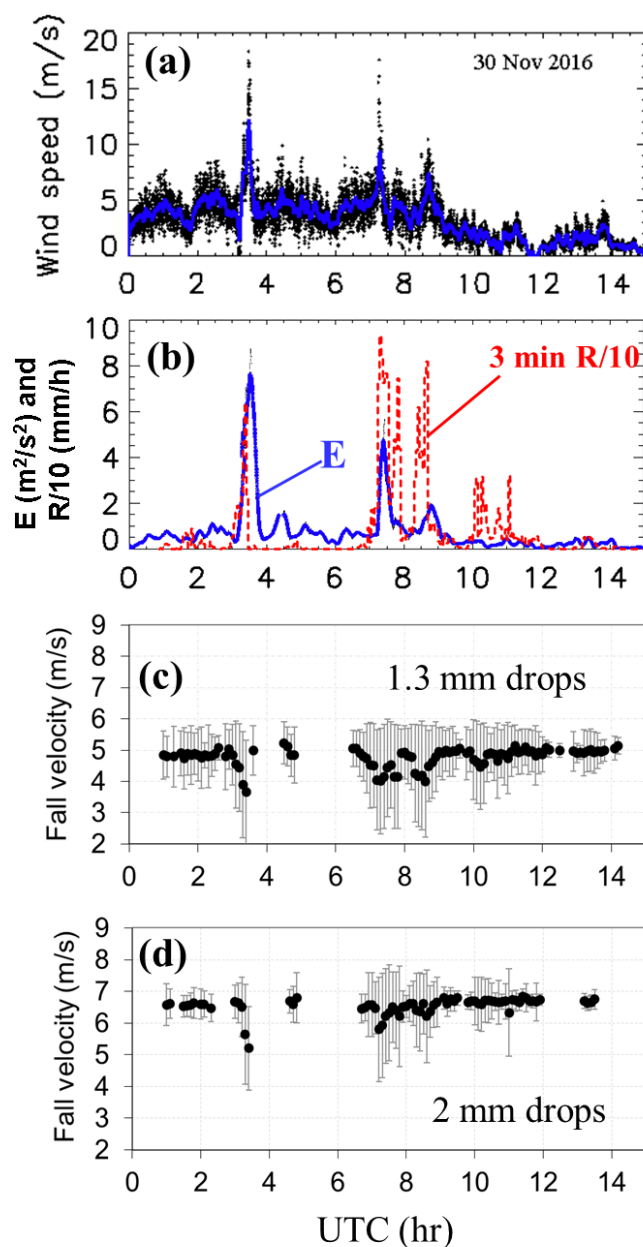
196 *Figure 3. (a) as in Fig. 1(a) except for 11 April 2016 event. The dashed line is fit to*
197 *Gunn-Kinzer at sea level. (b) as in Fig. 1(b) except for 11 April 2016 event.*

198

199 The second case considered is from 30 November 2016 wherein a supercell passed
200 over the instrumented site from 0300-0330 UTC producing about 15 mins later a long-
201 lived EF-2 tornado. Strong winds were recorded at the site with 5-min averaged speeds
202 reaching 10-12 m s⁻¹ between 0320-0330 and E values in the range to 7-8 m² s⁻²
203 indicating strong turbulence (Fig. 4a,b). The rain rates peaked at 70 mm h⁻¹ during this
204 time (Fig. 4b). About 3 h later several squall-line type storm cells passed over the site
205 from 0700-0900 UTC again with strong winds but considerably lower E values 2-4 m² s⁻²
206 and maximum R of 80 mm h⁻¹. After 1000 UTC the E values were much smaller (< 0.5
207 m² s⁻²) indicating calm conditions. The peak R is also smaller at 30 mm h⁻¹ at 1000 UTC.

208 Figure 4 panels (c) and (d) show the mean and $\pm 1\sigma$ of the fall speeds from the 2DVD
209 for the 1.3 and 2 mm drop sizes, respectively. The MPS data are not shown here since
210 during this event it was located outside the DFIR on its turntable and we did not want to
211 confuse the wind-effects between the two instruments. It is clear from Fig. 4(c) that
212 during the supercell passage (0300-0330 UTC) the mean fall speed for 1.3 mm drops
213 decreases (from 5 to 3.5 m s⁻¹) and the standard deviation increases (from 0.5 to 1.5 m
214 s⁻¹). The same trend can be seen for the subsequent squall-line rain cell passage from
215 0700-0900 UTC.

216



217

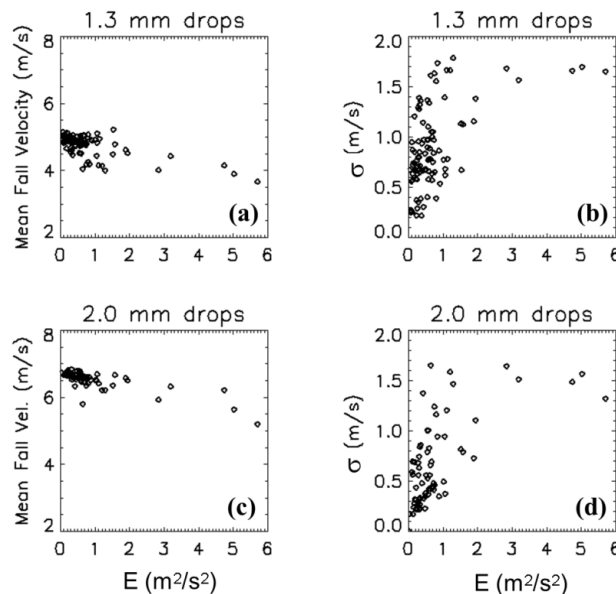
218 *Figure 4.* (a) as in Fig. 2(a) except for 30 Nov 2016 event. (b) as in Fig. 2(b). (c) mean
219 and $\pm 1\sigma$ standard deviation of fall speeds from 2DVD for 1.3 ± 0.1 mm sizes. (d) as in (c)
220 except for 2 ± 0.1 mm sizes.

221



222 To expand on this observed correlation, Fig. 5 (a,b) show scatterplots of the mean fall
223 speed and standard deviation versus E for the 1.3 mm drops (panels c and d show the
224 same but for the 2 mm drops). The mean fall speed decreases with increasing E nearly
225 linearly for $E > 1 \text{ m}^2 \text{ s}^{-2}$. This decrease relative to *Gunn-Kinzer* terminal fall speeds is
226 termed as “sub-terminal” and our data is in general agreement with (*Montero-Martinez*
227 *and Garcia-Garcia* 2016) who found an increase in the numbers of sub-terminal drops
228 with sizes between 1-2 mm under windy conditions using a 2D-Precipitation probe with
229 resolution of 200 microns (similar to 2DVD) but without wind fence. The standard
230 deviation of fall speeds (σ_f) versus E is shown in panels 6 (b,d). When $E > 1 \text{ m}^2 \text{ s}^{-2}$, the σ_f
231 is nearly constant at 1.5 m s^{-1} for both drop sizes. For $E < 1$, the σ_f is more variable and
232 essentially uncorrelated with E . From the discussion related to Fig. 1(b) and 3(b), σ_f
233 values exceeding 0.5 m s^{-1} can be attributed to physical as opposed to instrumental and
234 finite bin width effects. Thus, the fall speed distributions are considerably broadened
235 when $E > 1 \text{ m}^2 \text{ s}^{-2}$ due to increasing turbulence levels which is again consistent with the
236 findings of (*Montero-Martinez and Garcia-Garcia*, 2016) as well as (*Garrett and Yuter*,
237 2014). The latter observations, however, were of graupel fall speeds in winter
238 precipitation using a multi-angle snowflake camera (*Garrett et al.*, 2012).

239



240

241 *Figure 5.* (a,b) mean fall speed and standard deviation, respectively, versus E for 1.3
242 mm sizes. (c,d) same but for 2 mm sizes.

243



244 3 Discussion and Conclusions

245 We have reported on raindrop fall speed distributions using a high resolution (50
246 microns) droplet spectrometer (MPS) collocated with moderate resolution (170 microns)
247 2DVD to cover the entire size range (0.1 mm onwards) expected in natural rain. The
248 only comparable earlier study is by (*Montero-Martinez et al.*, 2009) who used collocated
249 2D-cloud and precipitation probes (2D-C, 2D-P) but restricted their data to calm wind
250 conditions. Their main conclusion was that the distribution of the ratio of the measured
251 fall speed to the terminal fall speed for 0.44 mm size, while having a mode at 1 was
252 strongly positively skewed with tails extending to 5 especially at high rain rates. In our
253 data shown in Fig. 1(b) and 3(b), there is no such strong positive skewness, and the
254 corresponding ratio does not exceed 2.

255 *Larsen et al.*, (2014) appear to confirm the ubiquitous existence of super-terminal fall
256 speeds for sizes < 1 mm using different instruments one of them being a 2DVD. It is
257 well-known that “mis-matched” drops cause erroneous fall speed estimates from 2DVD
258 for tiny drops. To clarify the “mis-matched” drop problem: it is very difficult to match a
259 drop detected in the top light-beam plane of the 2DVD to the corresponding drop in the
260 bottom plane for sizes < 0.5 mm (*Schoenhuber et al.*, 2008; Appendix in *Huang et al.*,
261 2010; *Bernauer et al.*, 2015). It is not clear if (*Larsen et al.*, 2014) accounted for this
262 problem in their analysis.

263 Our histograms of fall speeds for 1 mm sizes (Fig. 1b and 3b) under calm wind
264 conditions from both MPS and 2DVD did not show any evidence of either sub- or super-
265 terminal speeds, rather the histograms were symmetric with mean close to the Gunn-
266 Kinzer terminal velocity value. However, for the 0.5 mm sizes, our histogram of fall
267 speeds using the MPS under calm conditions cannot rule out the occurrence of both
268 sub- and super-terminal fall speeds, after accounting for instrumental and finite bin
269 width effects.

270 In a later study using only the 2D-P probe, (*Montero-Martinez and Garcia-Garcia*, 2016)
271 found sub-terminal fall speeds and broadened distributions under windy conditions for
272 1-2 mm sizes in general agreement with our results using 2DVD. *Stout et al.*, (1995)
273 simulated the motion of drops in isotropic turbulence and determined that there would
274 be a significant reduction of the average drop settling velocity (relative to terminal
275 velocity) of greater than 35% for drops around 2 mm size when the ratio of *rms* velocity
276 fluctuations (due to turbulence) relative to drop terminal velocity is around 0.8. Whereas
277 we did not have a direct measure of the *rms* velocity fluctuations, the proxy for
278 turbulence intensity (*E*) related to wind gusts during supercell passage (very large *E*
279 around 7 m² s⁻²) clearly shows a significant reduction in mean fall speeds of 25-30%
280 relative to terminal speed for 1.3 and 2 mm sizes with significant broadening of the fall
281 speed distributions relative to calm conditions.



282 When $E < 0.5-1 \text{ m}^2 \text{ s}^{-2}$, our data show that the mean fall speeds are within a few per cent
283 (<5%) of the *Gunn-Kinzer* terminal velocity over the entire range from 100 microns and
284 larger to precipitation sizes. For sizes $> 1 \text{ mm}$, no significant broadening of the fall
285 speed distribution over that ascribed to instrument and/or finite bin widths effects were
286 observed. While our dataset is limited to three events they cover a wind range of rain
287 rates, wind conditions and two different climatologies. Analysis of further events with
288 direct measurement of turbulent intensity would be needed to generalize our findings.

289

290 Data Availability

291 Data used in this paper can be accessed from:

292 ftp://lab.chill.colostate.edu/pub/kennedy/merhala/Bringi_et_al_2017_GRL_datasets/

293

294 Competing interests

295 VNB and MT declare they have no conflict of interest. DB is employed by Droplet
296 Measurements Technologies, Inc. located in Longmont, Colorado, USA who make the
297 Meteorological Particle Spectrometer used in this study.

298

299 Acknowledgements

300 Two of the authors (VNB and MT) acknowledge support from the U.S. National Science
301 Foundation via grant AGS-1431127. The assistance of Dr. Patrick Gatlin of
302 NASA/MSFC is gratefully acknowledged. Prof. Kevin Knupp and Mr. Carter Hulseley of
303 the University of Alabama in Huntsville processed the wind data.

304

305



306 References

- 307 Atlas, D., R. C. Srivastava, and R. S. Sekhon (1973). Doppler radar characteristics of
308 precipitation at vertical incidence, *Rev. Geophys.*, *11*, 1–35,
309 doi:<https://doi.org/10.1029/RG011i001p00001>
- 310 Barthazy, E., S. Göke, R. Schefold, and D. Högl (2004), An optical array instrument for
311 shape and fall velocity measurements of hydrometeors, *J. Atmos. Oceanic*
312 *Technol.*, *21*, 1400–1416, doi:[https://doi.org/10.1175/1520-](https://doi.org/10.1175/1520-0426(2004)021<1400:AOAIFS>2.0.CO;2)
313 [0426\(2004\)021<1400:AOAIFS>2.0.CO;2](https://doi.org/10.1175/1520-0426(2004)021<1400:AOAIFS>2.0.CO;2).
- 314 Baumgardner, D., Abel, S. J., Axisa, D., Cotton, R., Crosier, J., Field, P., Gurganus, C.,
315 Heymsfield, A., Korolev, A., Krämer, M., Lawson, P., McFarquhar, G., Ulanowski,
316 Z., and Um, J. (2017), Cloud Ice Properties: In Situ Measurement Challenges;
317 Chapter 9 of 'Ice Formation and Evolution in Clouds and Precipitation:
318 Measurement and Modeling Challenges', *Meteorol. Monographs*
319 doi:<https://doi.org/10.1175/AMSMONOGRAPHS-D-16-0011.1>, 2017.
320
- 321 Beard, K. V. (1976), Terminal velocity and shape of cloud and precipitation drops aloft,
322 *J. Atmos. Sci.*, *33*, 851–864, doi:[https://doi.org/10.1175/1520-](https://doi.org/10.1175/1520-0469(1976)033<0851:TVASOC>2.0.CO;2)
323 [0469\(1976\)033<0851:TVASOC>2.0.CO;2](https://doi.org/10.1175/1520-0469(1976)033<0851:TVASOC>2.0.CO;2)
- 324 Beard, K. V., and H. R. Pruppacher (1969), A determination of the terminal velocity and
325 drag of small water drops by means of a wind tunnel, *J. Atmos. Sci.*, *26*, 1066–
326 1072, doi: [https://doi.org/10.1175/1520-0469\(1969\)026<1066:ADOTTV>2.0.CO;2](https://doi.org/10.1175/1520-0469(1969)026<1066:ADOTTV>2.0.CO;2).
- 327 Belda, M., E. Holtanová, T. Halenka, and J. Kalvová (2014), Climate classification
328 revisited: From Köppen to Trewartha. *Climate Res.*, *59*, 1–13,
329 doi:<https://doi.org/10.3354/cr01204>.
- 330 Bernauer, F., K. Hürkamp, W. Rühm, and J. Tschiersch (2015), On the consistency of
331 2-D video disdrometers in measuring microphysical parameters of solid precipitation,
332 *Atmos. Meas. Tech.*, *8*, 3251–3261, doi: <https://doi.org/10.5194/amt-8-3251-2015>
- 333 Foote, G.B. and P.S. Du Toit (1969). Terminal Velocity of Raindrops Aloft. *J. Appl.*
334 *Meteor.*, *8*, 249–253, [https://doi.org/10.1175/1520-](https://doi.org/10.1175/1520-0450(1969)008<0249:TVORA>2.0.CO;2)
335 [0450\(1969\)008<0249:TVORA>2.0.CO;2](https://doi.org/10.1175/1520-0450(1969)008<0249:TVORA>2.0.CO;2)
- 336 Garrett, T. J., and S. E. Yuter (2014), Observed influence of riming, temperature, and
337 turbulence on the fallspeed of solid precipitation, *Geophys. Res. Lett.*, *41*, 6515–
338 6522, doi:10.1002/2014GL061016.
- 339 Garrett, T. J., Fallgatter, C., Shkurko, K., and Howlett, D. (2012), Fall speed
340 measurement and high-resolution multi-angle photography of hydrometeors in free fall,
341 *Atmos. Meas. Tech.*, *5*, 2625–2633, doi:10.5194/amt-5-2625-2012



- 342 Gunn, R. and G.D. Kinzer (1949). The terminal velocity of fall for water droplets in
343 stagnant air, *J. Meteor.*, 6, 243–248, [https://doi.org/10.1175/1520-0469\(1949\)006<0243:TTVOFF>2.0.CO;2](https://doi.org/10.1175/1520-0469(1949)006<0243:TTVOFF>2.0.CO;2)
- 345 Huang, G., V.N. Brinqi, and M. Thurai (2008). Orientation Angle Distributions of Drops
346 after an 80-m Fall Using a 2D Video Disdrometer, *J. Atmos. Oceanic
347 Technol.*, 25, 1717–1723, <https://doi.org/10.1175/2008JTECHA1075.1>
- 348 Huang, G., V.N. Brinqi, R. Cifelli, D. Hudak, and W.A. Petersen (2010). A Methodology
349 to Derive Radar Reflectivity–Liquid Equivalent Snow Rate Relations Using C-Band
350 Radar and a 2D Video Disdrometer, *J. Atmos. Oceanic Technol.*, 27, 637–
351 651, <https://doi.org/10.1175/2009JTECHA1284.1>
- 352 Joe, P., and R. List (1987). Testing and performance of two-dimensional optical array
353 spectrometer with grey scale, *J. Atmos. Oceanic Technol.*, 4, 139–150,
354 [https://doi.org/10.1175/1520-0426\(1987\)004<0139:TAPOTD>2.0.CO;2](https://doi.org/10.1175/1520-0426(1987)004<0139:TAPOTD>2.0.CO;2)
355
- 356 Knollenberg, R. (1970). The Optical Array: An alternative to scattering or extinction for
357 airborne particle size determination, *J. Appl. Meteorol.*, 9, 86–103,
358 doi:[https://doi.org/10.1175/1520-0450\(1970\)009<0086:TOAAAT>2.0.CO;2](https://doi.org/10.1175/1520-0450(1970)009<0086:TOAAAT>2.0.CO;2).
359
- 360 Knollenberg, R. (1976). Three new instruments for cloud physics measurements: The
361 2–D spectrometer probe, the forward scattering spectrometer probe and the active
362 scattering aerosol spectrometer, in International Conference on Cloud Physics,
363 American Meteorological Society, 554–561.,
364
- 365 Knollenberg, R. (1981). Clouds, Their Formation, Optical Properties and Effects, chap.
366 Techniques for probing cloud microstructure, Academic Press, edited by P.V.
367 Hobbs and A. Deepak. 495 pp
- 368 Korolev, A. V., Kuznetsov, S. V., Makarov, Y. E., and Novikov, V. S. (1991). Evaluation
369 of Measurements of Particle Size and Sample Area from Optical Array Probes, *J.
370 Atmos. Oceanic Tech.*, 8, 514–522, [https://doi.org/10.1175/1520-0426\(1991\)008<0514:EOMOPS>2.0.CO;2](https://doi.org/10.1175/1520-0426(1991)008<0514:EOMOPS>2.0.CO;2)
371
372
- 373 Korolev, A. V., J. W. Strapp, and G. A. Isaac (1998). Evaluation of the Accuracy of
374 PMS Optical Array Probes, *Journal of Atmospheric and Oceanic Technology*, 15,
375 708–720, [https://doi.org/10.1175/1520-0426\(1998\)015<0708:EOTAOP>2.0.CO;2](https://doi.org/10.1175/1520-0426(1998)015<0708:EOTAOP>2.0.CO;2)
376
- 377 Korolev, A. V. (2007). Reconstruction of the Sizes of Spherical Particles from Their
378 Shadow Images. Part I: Theoretical Considerations, *Journal of Atmospheric and
379 Oceanic Technology*, 24, 376–389, <https://doi.org/10.1175/JTECH1980.1>
- 380 Larsen, M.L., A.B. Kostinski, and A.R. Jameson (2014). Further evidence for super
381 terminal drops, *Geophysical Research Letters*, 41, 2014GL061397.



- 382 List, R., N.R. Donaldson, and R.E. Stewart (1987). Temporal Evolution of Drop Spectra
383 to Collisional Equilibrium in Steady and Pulsating Rain, *J. Atmos. Sci.*, *44*, 362–
384 372, [https://doi.org/10.1175/1520-0469\(1987\)044<0362:TEODST>2.0.CO;2](https://doi.org/10.1175/1520-0469(1987)044<0362:TEODST>2.0.CO;2)
- 385 Löffler-Manq, M. and J. Joss (2000), An Optical Disdrometer for Measuring Size and
386 Velocity of Hydrometeors, *J. Atmos. Oceanic Technol.*, *17*, 130–
387 139, [https://doi.org/10.1175/1520-0426\(2000\)017<0130:AODFMS>2.0.CO;2](https://doi.org/10.1175/1520-0426(2000)017<0130:AODFMS>2.0.CO;2)
- 388 Montero-Martinez, G. and F. Garcia-Garcia (2016), On the behavior of raindrop fall
389 speed due to wind, *Quarterly Journal of the Royal Meteorological Society*, *142*,
390 2794, DOI: 10.1002/qj.2794.
- 391 Montero-Martinez, G., A. B. Kostinski, R. A. Shaw, and F. Garcia-Garcia (2009), Do all
392 raindrops fall at terminal speed?, *Geophysical Research Letters*, *36*, 246 L11818,
393 doi:10.1029/2008GL037111.
- 394 Notaroš, B., V. N. Bringi, C. Kleinkort, P. Kennedy, G-J Huang, M. Thurai, A. J.
395 Newman, W. Bang and G. Lee (2016), Accurate Characterization of Winter
396 Precipitation Using Multi-Angle Snowflake Camera, Visual Hull, Advanced
397 Scattering Methods and Polarimetric Radar, *Atmosphere*, *7*(6), 81;
398 doi:10.3390/atmos7060081
- 399 Rasmussen, R., B. Baker, J. Kochendorfer, T. Meyers, S. Landolt, A.P. Fischer, J.
400 Black, J.M. Thériault, P. Kucera, D. Gochis, C. Smith, R. Nitu, M. Hall, K. Ikeda,
401 and E. Gutmann (2012), How Well Are We Measuring Snow: The
402 NOAA/FAA/NCAR Winter Precipitation Test Bed. *Bull. Amer. Meteor.*
403 *Soc.*, *93*, 811–829, <https://doi.org/10.1175/BAMS-D-11-00052.1>
- 404 Rosewell, C.J. (1986). Rainfall Kinetic Energy in Eastern Australia, *J. Climate Appl.*
405 *Meteor.*, *25*, 1695–1701, [https://doi.org/10.1175/1520-0450\(1986\)025<1695:RKEIEA>2.0.CO;2](https://doi.org/10.1175/1520-0450(1986)025<1695:RKEIEA>2.0.CO;2)
- 407 Schönhuber, M., Günter Lammer, Randeu W.L. (2007), *Advances in Geosciences*, *10*,
408 pp. 85-90, 2007, <https://doi.org/10.5194/adgeo-10-85-2007>.
- 409 Schönhuber, M., G. Lammar, and W. L. Randeu (2008), “The 2D-video-distrometer”,
410 Chapter 1 in “Precipitation: Advances in Measurement, Estimation and Prediction”,
411 S. C. Michaelides, Ed., Springer, 3–31.
- 412 Sekhon, R.S. and R.C. Srivastava (1971), Doppler Radar Observations of Drop-Size
413 Distributions in a Thunderstorm, *J. Atmos. Sci.*, *28*, 983–994,
414 [https://doi.org/10.1175/1520-0469\(1971\)028<0983:DROODS>2.0.CO;2](https://doi.org/10.1175/1520-0469(1971)028<0983:DROODS>2.0.CO;2)
- 415 Stout, J.E., S.P. Arya, and E.L. Genikhovich (1995), The Effect of Nonlinear Drag on the
416 Motion and Settling Velocity of Heavy Particles, *J. Atmos. Sci.*, *52*, 3836–3848,
417 [https://doi.org/10.1175/1520-0469\(1995\)052<3836:TEONDO>2.0.CO;2](https://doi.org/10.1175/1520-0469(1995)052<3836:TEONDO>2.0.CO;2)



- 418 Testik, F.Y. and M.K. Rahman (2016). High-Speed Optical Disdrometer for Rainfall
419 Microphysical Observations, *J. Atmos. Oceanic Technol.*, 33, 231–243,
420 <https://doi.org/10.1175/JTECH-D-15-0098.1>
- 421 Thériault, J.M., R. Rasmussen, E. Petro, J. Trépanier, M. Colli, and L.G. Lanza
422 (2015), Impact of Wind Direction, Wind Speed, and Particle Characteristics on the
423 Collection Efficiency of the Double Fence Intercomparison Reference, *J. Appl.*
424 *Meteor. Climatol.*, 54, 1918–1930, <https://doi.org/10.1175/JAMC-D-15-0034.1>
- 425 Thurai, M. and V. N. Bringi (2005), Drop axis ratios from a 2D video disdrometer, *J.*
426 *Atmos. Oceanic Technol.*, 22, 966–978, <https://doi.org/10.1175/JTECH1767.1>
- 427 M. Thurai, V. N. Bringi, M. Szakáll, S. K. Mitra, K. V. Beard, and S. Borrmann (2009),
428 Drop Shapes and Axis Ratio Distributions: Comparison between 2D Video
429 Disdrometer and Wind-Tunnel Measurements, *Journal of Atmospheric and*
430 *Oceanic Technology*, 26 (7), 1427–1432,
431 <https://doi.org/10.1175/2009JTECHA1244.1>
- 432 Thurai, M., V. N. Bringi, W. A. Petersen, P. N. Gatlin (2013), Drop shapes and fall
433 speeds in rain: two contrasting examples, *J. Appl. Meteor. Climatol.*, 52,
434 2567–2581, <https://doi.org/10.1175/JAMC-D-12-085.1>
- 435 Thurai, M., P. Gatlin, V. N. Bringi, W. Petersen, P. Kennedy, B. Notaroš, and L. Carey
436 (2017), Toward completing the raindrops size spectrum: Case studies involving
437 2D-video disdrometer, droplet spectrometer, and polarimetric radar measurements,
438 *J. Appl. Meteor. Climatol.*, 56, 877–896, <https://doi.org/10.1175/JAMC-D-16-0304.1>
- 439 Trewartha, G. T., and L. H. Horn (1980), *Introduction to Climate*, 5th ed. McGraw Hill,
440 416 pp.